

Measurement of Material Thickness Using X-ray Attenuation

By

Oliver Mikhail H. Gaerlan

A Thesis
Submitted to the Faculty of
Mississippi State University
in Partial Fulfillment of the Requirements
for the Degree of Bachelor of Science
in Physics
in the Department of Physics and Astronomy

Mississippi State, Mississippi

April 2016

Measurement of Material Thickness Using X-ray Attenuation

By

Oliver Mikhail H. Gaerlan

Approved:

James A. Dunne
(Major Professor)

Dipangkar Dutta
(Committee Member)

Seth F. Oppenheimer
(Committee Member)

ACKNOWLEDGEMENTS

I would like to thank Dr. Dutta for giving me the opportunity to conduct research with him since my senior year at the Mississippi School for Mathematics and Science.

I thank my parents for financially supporting me throughout my undergraduate career.

I thank my committee for their comments on this thesis, and I thank Dr. James A. Dunne for directing this research.

TABLE OF CONTENTS

DEDICATION	ii
ACKNOWLEDGEMENTS	iii
LIST OF TABLES	vi
LIST OF FIGURES	vii
LIST OF SYMBOLS, ABBREVIATIONS, AND NOMENCLATURE	viii
CHAPTER	
1. INTRODUCTION	1
1.1 Motivation	1
1.2 Experiment Overview	2
2. THEORY AND BACKGROUND	3
2.1 Radiation	3
2.2 Photon Interactions	3
2.3 Attenuation	5
2.4 X-ray Production and Detection	7
2.5 Least Squares	9
3. EXPERIMENT	11
3.1 Safety	11
3.2 Apparatus	13
3.3 Intensity Measurements	16
3.4 Physical Measurements	19
4. ANALYSIS	25
4.1 Preliminary Data	25

4.2	Data Modeling	26
4.3	Intensity Calculations	30
4.4	Physical Measurements	30
4.5	Attenuation Coefficients	31
4.5.1	Mass Attenuation Coefficients	32
4.5.2	Monte Carlo Calculation	32
4.6	Thin Foil Measurements	34
5.	CONCLUSION	35
5.1	Summary	35
5.2	Future Work	36
	REFERENCES	37
	APPENDIX	
A.	APPARATUS DIMENSIONS	37
A.1	Apparatus Dimensions	38

LIST OF TABLES

3.1	Percent weight composition of AL7075-T6	17
3.2	Sample data file	20
3.3	Sample graphs of the source from data set 1	21
3.4	Source trial 1 data for old and new configurations	22
3.5	Summary of data sets	22
3.6	Area measurements	23
3.7	Mass measurements	24
3.8	Thick foil measurements	24
4.1	Models for source trial 1	28
4.2	Model parameters and standard errors for source trial 1 Gaussian models	29
4.3	Model parameters and standard errors for source trial 1 cubic models	29
4.4	Intensity measurements for data set 5	31
4.5	Attenuation coefficients for elements in AL7075-T6	33

LIST OF FIGURES

2.1	Cross section of Al as a function of energy	6
2.2	Decay scheme of Am ²⁴¹	8
3.1	Dosimeter	12
3.2	Apparatus overview with construction guidelines	14
3.3	a) Outside view of the shielding enclosure while open. b) The detector inside the shielding enclosure.	15
3.4	Preparation of the experiment	18
3.5	Experimental setup within the detector	18
4.1	Monte Carlo calculation of mass attenuation coefficient for AL7075-T6	33
A.1	Base dimensions	39
A.2	Collimator dimensions	40
A.3	Source holder dimensions	41
A.4	Window dimensions	42

LIST OF SYMBOLS, ABBREVIATIONS, AND NOMENCLATURE

This section is optional, and may be formatted in an appropriate manner. The title `\listofsymbolsname` may be redefined as needed.

JLab Thomas Jefferson National Accelerator Facility (Jefferson Lab)

amu atomic mass units

Am²⁴¹ An isotope of the element Americium with an atomic weight of 241 amu

Al Aluminum

ALARA As Low As Reasonably Achievable

Ge Germanium

ICET Institute of Clean Energy Technology

NIST National Institute of Standards and Technology

Np²³⁷ An isotope of the element Neptunium with an atomic weight of 237

Research Park Thad Chocran Research, Technology, and Economic Development Park

eV electron volt - the amount of energy required to move an electron in a potential difference of one volt

CHAPTER 1

INTRODUCTION

1.1 Motivation

The QWeak experiment, which ran at the Thomas Jefferson National Accelerator Facility in Newport News, Virginia, was designed to accurately measure the proton's weak charge. The weak charge is the neutral current analog of the electromagnetic charge of the proton. It is measured by finding the difference in the scattering of differently polarized electron beams aimed at a proton target.

The proton target was contained in an aluminum container with thin aluminum windows which the electron beam traveled through. For the final analysis of the experiment, the thickness of the aluminum windows needed to be measured. The thickness of these aluminum windows were on the order of a few mils and curved in shape so traditional physical measurements were not feasible. X-ray measurements allow for minimal physical interference with the window during measurements.

Adesh Subedi, a recent applied physics Ph.D. graduate from MSU, conducted this experiment at JLab with a different setup than the one described in this thesis. His measurements for the thicknesses using x-ray attenuation yielded inconsistent results and were subsequently not used in his final analysis. A sample window from JLab was sent to MSU for use in this experiment to repeat the experiment with a better setup.

1.2 Experiment Overview

The experiment will measure the thickness of a thin aluminum foil by sending a beam of x-rays through the foil. The thickness of the foil is related to the difference in the intensity of x-rays that pass through the aluminum window and the initial intensity of the x-ray source. The intensity is also related to a property of the material known as its attenuation coefficient. To calculate the attenuation coefficient, another foil with known thickness, mass, and surface density is used to calculate the attenuation coefficient. This is required even though the attenuation coefficients have been measured for most of the elements because the window is an aluminum alloy and the exact composition is somewhat uncertain.

The photoelectric effect is the absorption of a photon into an atom and the subsequent ejection of an electron that was bounded by the atom. The energy of the ejected electron, E , is given by the equation

$$E = h\nu - \phi \quad (2.1)$$

where h is Planck's constant, ν is the frequency of the photon and ϕ is the binding energy of the electron. Since bounded electrons have discrete binding energies, the photoelectric cross section as a function of the energy of the photon show jumps that correspond to different shells in the atom.

Compton scattering is the interaction of photons with free, or in this experiment, atomic electrons, where the photon only loses some of its energy. The photon scatters off the electron and has the relation

$$\cot(\phi) = (1 + \gamma) \tan\left(\frac{\theta}{2}\right) \quad (2.2)$$

$$\text{where } \gamma = \frac{h\nu}{m_e c^2} \quad (2.3)$$

and h is Planck's constant, ν is the frequency of the photon, m_e is the mass of an electron, c is the speed of light, θ is the photon's scattering angle and ϕ is the recoiling electron's scattering angle.

Pair production is a process that converts a photon into an electron-positron pair in the presence of a nucleus. However, this process only occurs above photon energies of 1.022 MeV. [cite NPP book]

the pair production in the field of atomic electrons, and σ_{phn} is the cross section due to the photonuclear effect. Figure 2.1 shows an image of the cross section as a function of photon energy. In the energy range of interest, the photoelectric and Compton effects dominate. [cite NIST]

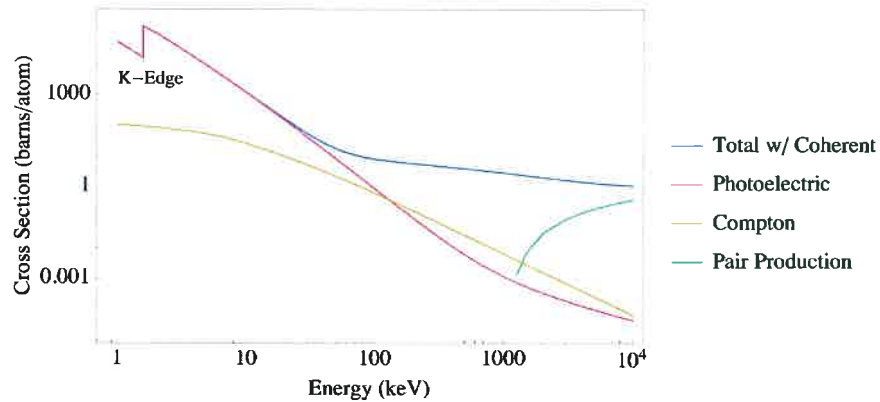


Figure 2.1

Cross section of Al as a function of energy

The linear attenuation coefficient, as opposed to the mass attenuation coefficient, is what is usually measured experimentally, but the linear attenuation is also directly proportional to the density of the material that the photons pass through. Since photons interact with the electrons, the attenuation coefficient is related to the electron density which is also related to the bulk density. The intensity formula can be re-written in terms of μ_{ℓ} such that

$$I = I_0 e^{-\mu_{\ell} t} \quad (2.7)$$

where μ_{ℓ} is the linear attenuation coefficient. Thus when measuring the attenuation coefficients between two materials of the same composition, differences in density may cause

If Np^{237} is bombarded by x-rays, the resulting collision may knock out K-shell ($n = 1$) electrons resulting in the gaps being filled by higher state electrons and will release the energy in the form of x-rays. The three most common transitions are from $n = 3$ to $n = 2$, $n = 5$ to $n = 2$, and $n = 5$ to $n = 2$ which correspond to energies of 13.9 keV, 17.8 keV, and 20.8 keV respectively. Figure 2.2 shows a decay scheme of Am^{241} into Np^{237} .

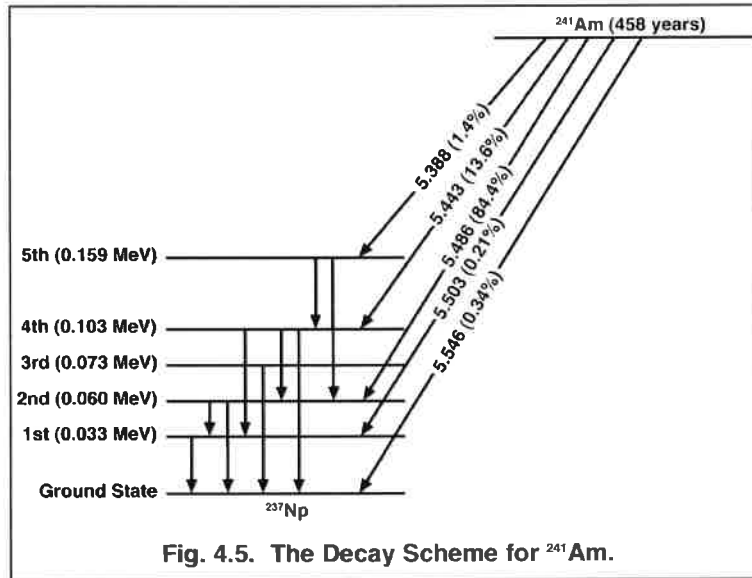


Figure 2.2

Decay scheme of Am^{241}

The x-rays that exit the source and enter the detector are then absorbed by a high-purity germanium crystal. The resulting energy is measured by determining the total electric charge detected in the crystal. Above 15 keV, the x-rays interact with the germanium via the photoelectric effect.[cite x-ray document]

where λ is some damping factor, δ is the increment between solutions, and I is the identity matrix. The Levenberg-Marquardt algorithm provides a more robust method to find a minimum. [cite numerical book]

rial must be conducted at designated areas only, so the majority of this experiment was conducted in a laboratory in the Energy Institute at the Research Park.

The main concept of radiation safety is the acronym ALARA (As Low As Reasonably Achievable). Since radiation exposure is completely impossible to avoid, the aim is simply to reduce the amount of exposure as much as possible. The amount of exposure is typically measured by a device called a dosimeter. The dosimeter used during this experiment, shown in Figure 3.1, was in the shape of a small badge that attaches to the torso.



Figure 3.1

Dosimeter

Radiation exposure can be measured in a number of units. Common units include grays, rads, sieverts, and rems. A gray is the SI unit of absorbed dose and is equal to an absorbed dose of one joule per kilogram. A rad is simply 0.01 grays. A sievert is the SI unit of dose equivalent and is equal to absorbed dose in gray times some quality factor which depends on the type of radiation. Similarly, a rem is equivalent to 0.01 sieverts. Radiation occurs naturally and from also everyday manmade objections. The average human receives

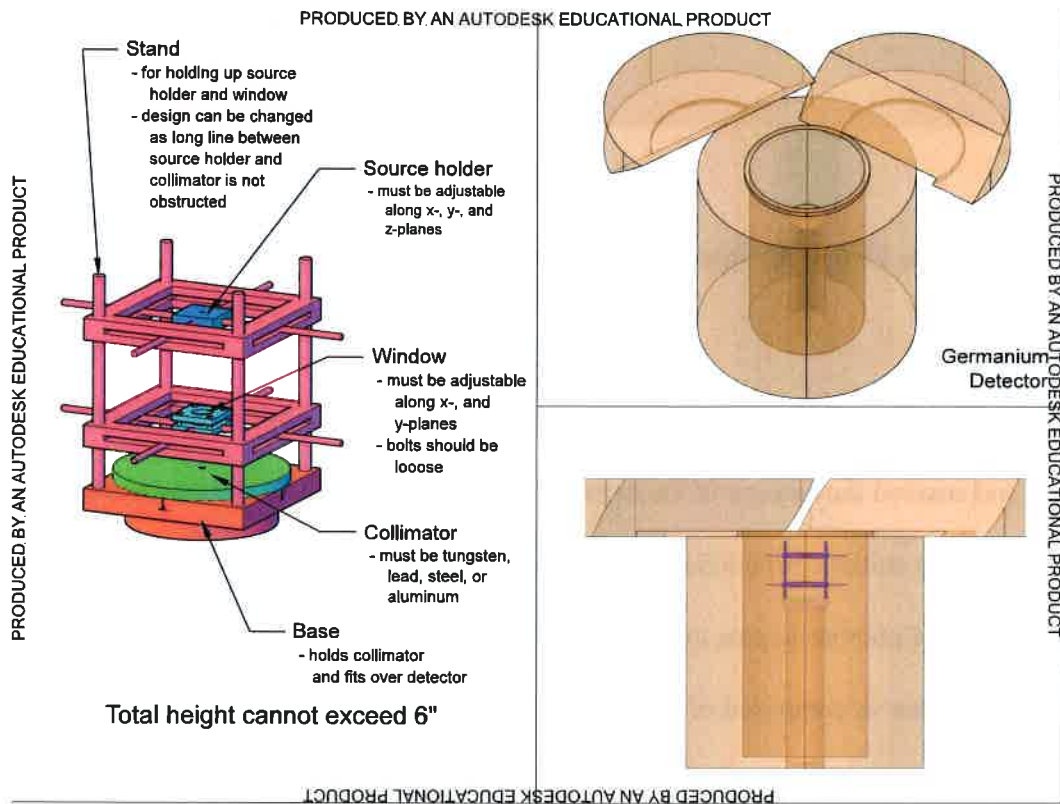


Figure 3.2

Apparatus overview with construction guidelines

less steel capsule with a small window at one of the bases. The depth of the source holder hole was designed to be slightly less thick than the length of the capsule such that dead end of the source would stick out of the top for easy removal between runs. A small lip at the bottom of the hole of the source holder would keep the source in place.

The stand was designed to hold the window and the source holder. The window and the source holder both needed to be adjustable in three dimensions so that the three components could be adjusted to align the photon beam. The stand is comprised of four long threaded rods with two hollow square bases that hold the window and source holder. Each square base is attached to the four threaded rods through holes in each corner of the bases. Bolts were used to secure each square base at some fixed height along the stand. The square bases also had slits on each side that would hold smaller screws so that the window and source holder could be adjusted along the horizontal plane.

Design details are shown in Appendix A. Once the design was complete, a schematic of the apparatus was sent to the machine shop at ICET to be built.

3.3 Intensity Measurements

Several sets of data were gathered at ICET by Ron Unz over the course of several weeks. The radioactive source and the entire apparatus was housed at ICET in a radiologically controlled room during the duration of the experiment.

There were two target materials: a thick foil and a thin foil. Both foils are made of the same aluminum alloy, AL7075-T6. The percent weight composition of AL 7075-T6 is given in Table 3.1. The thin foils's thickness would be indirectly calculated using the mass



Figure 3.4

Preparation of the experiment



Figure 3.5

Experimental setup within the detector

Table 3.2

Sample data file

\$SPEC.ID:
Molnar Range
\$SPEC.REM:
DET# 1
DETDESC# HPGe Detector 1
AP# GammaVision Version 6.07
\$DATE.MEA:
10/19/2015 09:56:53
\$MEAS.TIM:
3600 3733
\$DATA:
0 8191
0
0
:
0
0
0
\$ROI:
0
\$PRESETS:
Live Time
3600
0
\$ENER.FIT:
0.137869 0.366631
\$MCA.CAL:
3
1.378689E-001 3.666307E-001 -4.415950E-008 keV
\$SHAPE.CAL:
3
2.301834E+000 9.195991E-004 -5.357180E-008

Table 3.4

Source trial 1 data for old and new configurations

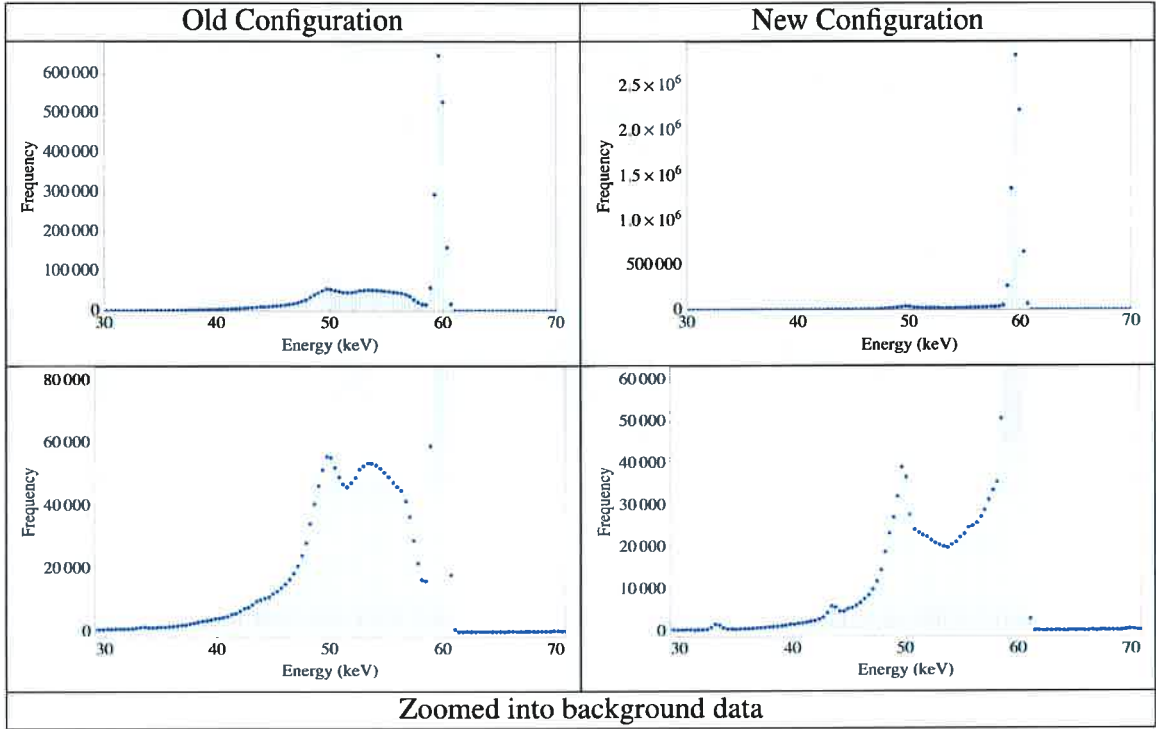


Table 3.5

Summary of data sets

Data Set	1	2	3	4	5
Configuration	old	old	old	new	new
Live Time (h)	1	1	1	1	24
Number of Trials					
Source	2	2	2	2	2
Thick Foil	1	1	1	2	2
Thin Foil	1	1	1	2	2

Table 3.7

Mass measurements



	Trial	Mass (g)
	1	1.5358
	2	1.5356
	3	1.5354
	4	1.5356
	5	1.5354
	6	1.5354
	7	1.5354
	8	1.5354
	9	1.5354
Precision Scale	10	1.5354

Table 3.8

Thick foil measurements

	Trial	Data Set 1 Thickness (mm)	Data Set 2 Thickness (mm)	Data Set 3 Thickness (mm)
	1	0.8876	0.8857	0.8805
	2	0.8850	0.8870	0.8886
	3	0.8803	0.8719	0.8953
	4	0.8712	0.8722	0.8966
	5	0.8849	0.8868	0.8818
	6	0.8931	0.8839	0.8950
	7	0.8946	0.8923	0.8886
	8	0.8916	0.8919	0.8749
	9	0.8880	0.8884	0.8922
	10	0.8909	0.8885	0.8908
	11	0.8936	0.8909	0.8837
	12	0.8884	0.8851	0.8716
	13	0.8856	0.8838	0.8689
	14	0.8831	0.8891	0.8760
	15	0.8927	0.8844	0.8868
Precision Micrometer	16	0.8871	0.8756	8.8842

Before analysis, the data needed to be corrected for deadtime. The deadtime is due to the amount of time the detector takes to record an event. Any events during the dead time are not recorded. The deadtime was calculated with the following formula

$$DT = \frac{LT - RT}{RT} \quad (4.2)$$

where DT is the dead time, LT is the live time, and RT is the real time. The run time and the live time are located under the \$MEAS_TIM: line in the data file. The first number corresponds to the run time, and the second corresponds to the live time. The corrections for each data point then is

$$\text{correction} = \frac{\text{count}}{1 - DT} \quad (4.3)$$

where count is the data point and correction is the corrected data point.

4.2 Data Modeling

After the data points have been corrected, the data needed to be modeled. The frequency was modeled against the energy. There were two main components of the data: the background and the peak. The peak is the most prominent feature of the data and can be modeled by a Gaussian curve with the formula

$$f(x; p, \mu, \sigma) = p e^{-\frac{1}{2}\left(\frac{x-\mu}{\sigma}\right)^2} \quad (4.4)$$

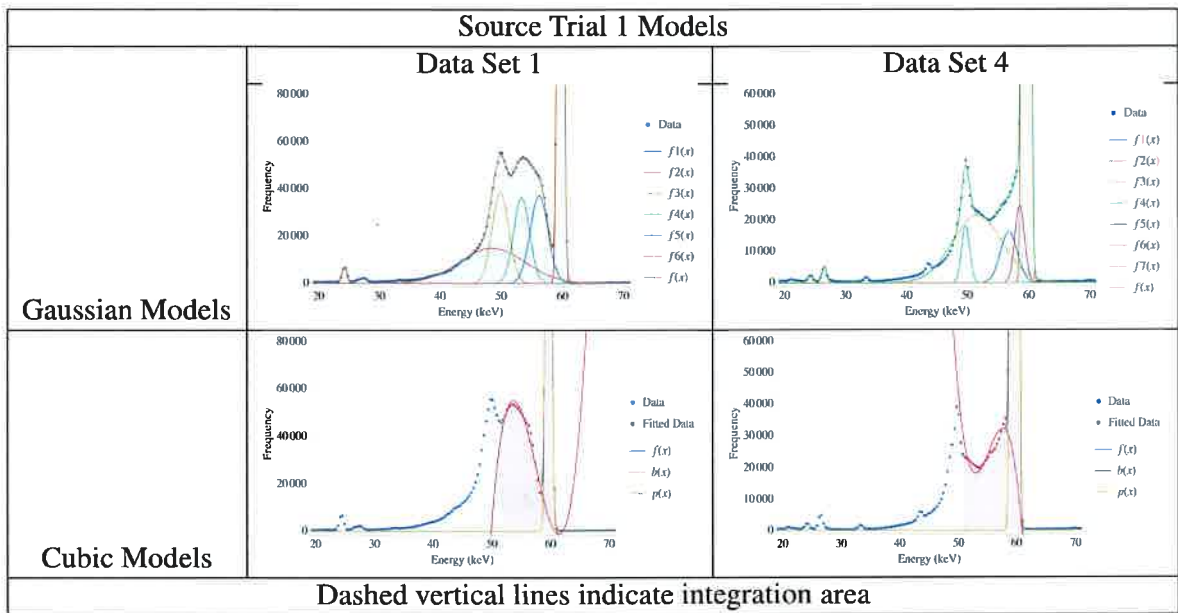
where p is the height of the peak, μ is the center, and σ is the standard deviation.

The background was fitted with two different models: a cubic polynomial and a sum of Gaussians. The cubic polynomial used the formula

$$b(x; a, b, c, d) = ax^3 + bx^2 + cx + d \quad (4.5)$$

Table 4.1

Models for source trial 1



4.3 Intensity Calculations

Once a general model for the data was obtained, the peak was singled out from the background. The peak model was integrated to find the intensity. That is,

$$I = \int_{-\infty}^{\infty} f_p(x) dx = p_p \sigma_p \sqrt{2\pi} \quad (4.8)$$

$$\approx \int_{\mu-2FWHM}^{\mu+2FWHM} f_p(x) dx \quad (4.9)$$

where $FWHM$ is the full-width-half-maximum and is given by the formula

$$FWHM = 2\sigma\sqrt{2\pi}. \quad (4.10)$$

The error was calculated using the formula

$$\sigma_I^2 = \sum_i \sigma_{f_p(x_i)}^2 \quad (4.11)$$

$$\text{where } \sigma_{f_p(x_i)}^2 = \sigma_{\mu_p}^2 \left(\frac{\partial f_p}{\partial \mu_p} \right)_{x_i}^2 + \sigma_{\sigma_p}^2 \left(\frac{\partial f_p}{\partial \sigma_p} \right)_{x_i}^2 + \sigma_{p_p}^2 \left(\frac{\partial f_p}{\partial p_p} \right)_{x_i}^2 + \sigma_{x_i}^2 \left(\frac{\partial f_p}{\partial x_i} \right)_{x_i}^2 \quad (4.12)$$

where σ_j is the error associated with the j parameter or variable and x_i is from $\mu_p - 2FWHM$ to $\mu_p + 2FWHM$. A summary of the intensity measurements for data set 5 is shown in Table 4.4.

4.4 Physical Measurements

The average of the mass trials yielded a measurement of 1.5348(14) g. The area was calculated using the formula

$$A = \frac{1}{2} \sum_{k=1}^{n-1} (x_{k+1} + x_k) (y_{k+1} - y_k) \quad (4.13)$$

which is for an arbitrary n -polygon whose vertices have coordinates (x_k, y_k) . Each vertex measurement had an error of 0.5 μm , and by using a Monte Carlo simulation with 5,000

4.5.1 Mass Attenuation Coefficients

The mass attenuation coefficient for each data set could be calculated using the data from the physical measurements of the thick foil. By Equation 2.4, the mass attenuation coefficient, μ , was found using

$$\mu = \frac{\ln(I_0) - \ln(I)}{M/A} \quad (4.14)$$

where I is the intensity of the thick foil, I_0 is the intensity of the source, M is the mass of the thick foil, and A is the area of the thick foil.

For each data set, the attenuation coefficients were calculated using every combination of trials of the source and thick foil data. The mass attenuation coefficient using data set 5 was calculated to be $0.3878(4) \text{ cm}^2/\text{g}$ with a 0.090% error.

4.5.2 Monte Carlo Calculation

A theoretical value for the mass attenuation coefficient could be calculated using a Monte Carlo method. By the central limit theorem, the probability distribution of the mass attenuation coefficients should converge to a normal distribution for any distribution of the variables, so a uniform distribution for each element in the ranges shown in Table 3.1 was used for the Monte Carlo method. The NIST values for the mass attenuation coefficients for each element at 60 keV shown in Table 4.5 were used for the calculations.

1,000,000 trials were generated, and for each trial, a mass attenuation coefficient was calculated using Equation 2.8. Then a Gaussian model was fitted to a histogram of the data as shown in Figure 4.1. The mean was found to be $0.387(6) \text{ cm}^2/\text{g}$ with a 1.5% error.

4.6 Thin Foil Measurements

From Equation 2.7, the thickness of the thin foil, t , can be calculated with the equation

$$t = T \frac{\ln(I_2) - \ln(I_0)}{\ln(I_1) - \ln(I_0)} \quad (4.15)$$

where T is the thickness of the thick foil, I_0 is the intensity of the source, I_1 is the intensity with the thick foil, and I_2 is the intensity with the thin foil. Using data set 5, there were two distinct thickness measurements of 94.2(8) μm and 80.8(7) μm when using trial 1 and trial 2 thin intensities respectively which correspond to 3.71(3) mil and 3.18(3) mil and 0.86% and 0.90% percent error.

5.2 Future Work

Suggestions for improvement include increasing the lip thickness to produce a more narrow beam from the source holder. A better way to precisely align the source holder, window, and collimator also needs to be designed.

A Geant simulation will be written in the future to model the entire experiment. Geant is a software kit developed by CERN for the “simulation of the passage of particles through matter.” This simulator hopefully will be able to explain some of the shapes in the background and the effects of the placement of the materials within the apparatus.

A.1 Apparatus Dimensions

The first figure shows the overall configuration of the apparatus along with construction guidelines for the machine shop. The next few figures show the specific shapes and dimensions of each part of the apparatus.

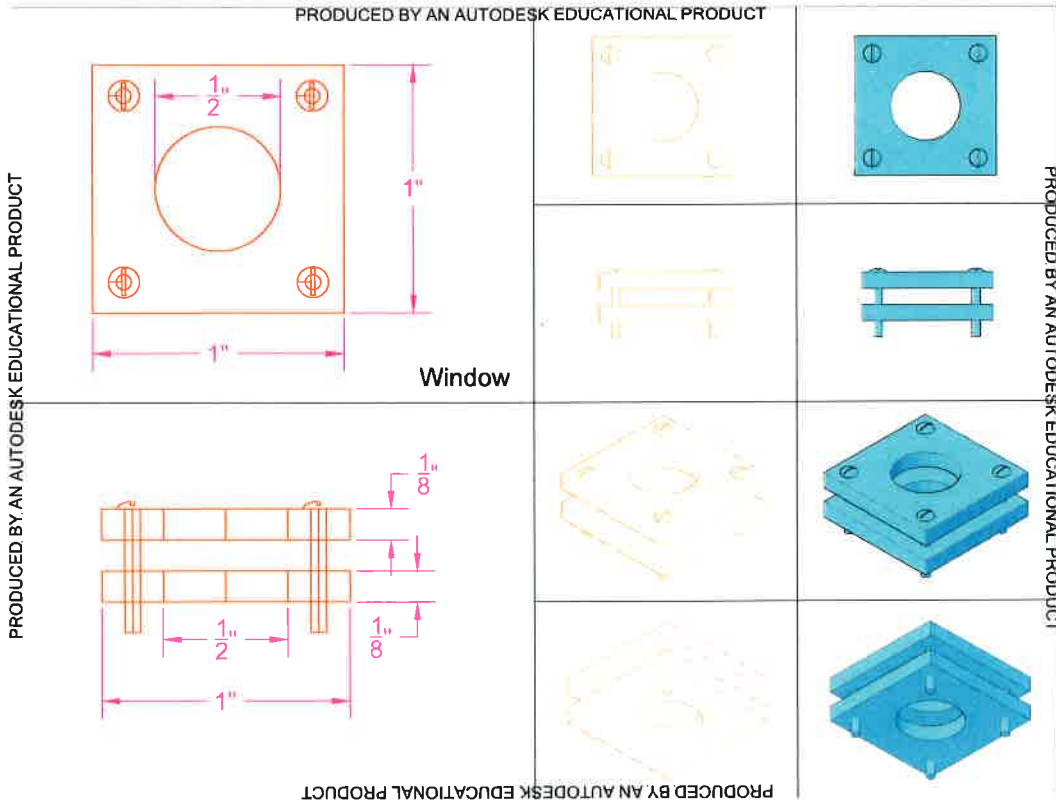


Figure A.4
Window dimensions